# Role of 14-3-3 proteins in human cardiac sodium channel $Na_v1.5$ regulation

Oksana Iamshanova[1], Anne-Flore Hämmerli[1], Elise Ramaye[1], Arbresh Seljmani[1,2], Daniela Ross-Kaschitza[1], Noëlia Schärz[1,2], Maria Essers[1], Sabrina Guichard[1], Jean-Sebastien Rougier[1], Hugues Abriel[1]

[1] - Institute of Biochemistry and Molecular Medicine and Swiss National Center of Competence in Research (NCCR) TransCure, University of Bern, Bern, Switzerland

[2] - medi - Center for Medical Education, Bern, Switzerland

Correspondence: oksana.iamshanova@ibmm.unibe.ch

hugues.abriel@ibmm.unibe.ch

## Abstract

**Background:** 14-3-3 proteins are ubiquitous proteins that play a role in cardiac physiology (*e.g.*, metabolism, development, and cell cycle). Furthermore, 14-3-3 proteins were proposed to regulate the electrical function of the heart by interacting with several cardiac ion channels, including the voltage-gated sodium channel $Na_v1.5$. Given the many cardiac arrhythmias associated with $Na_v1.5$ dysfunction, understanding its regulation by the protein partners is crucial.

**Aims:** In this study, we aimed to investigate the role of 14-3-3 proteins in the regulation of the human cardiac sodium channel $Na_v1.5$.

**Methods and Results:** Amongst the seven 14-3-3 isoforms, only 14-3-3η (encoded by *YWHAH*) co-immunoprecipitated with $Na_v1.5$ when heterologously co-expressed in tsA201 cells. Total and cell surface expression of $Na_v1.5$ was however not modified by 14-3-3η overexpression or inhibition with difopein, and 14-3-3η did not affect physical interaction between $Na_v1.5$ α-α subunits. The amplitude of $Na_v1.5$-mediated sodium peak current density significantly increased upon co-expression with difopein.

**Conclusions:** Our findings illustrate that the direct implication of 14-3-3 in regulating $Na_v1.5$ is not evident in the heterologous expression system used here. Potentiation of $Na_v1.5$-mediated current by difopein could be explained by the inhibition of 14-3-3/ligand interactions with other partner proteins of the channel complex (*e.g.*, PKA, PKC, CaMKII) and should be further investigated.

## Keywords

Voltage-gated sodium channel; $Na_v1.5$; 14-3-3 protein; difopein; channelosome; macromolecular complex

## Introduction

Voltage-gated sodium channel, $Na_v1.5$ (encoded by *SCN5A*), is responsible for the propagation of the action potential in the contractile myocardium. The function of $Na_v1.5$ largely relies on the interaction with its protein partners that regulate proper localization, turnover, and biophysical properties of the channel [1]. Dysfunction of $Na_v1.5$ is associated with various lethal diseases such as cardiac arrhythmias and cardiomyopathy. Therefore, understanding the relationship between $Na_v1.5$ and its regulatory protein partners may uncover novel therapeutic strategies for patients suffering from *SCN5A*-related diseases.

One of the protein partners of $Na_v1.5$ was reported to be 14-3-3 proteins, which are a family of conserved regulatory molecules expressed in all eukaryotic cells. 14-3-3 can bind target proteins, modulating protein-protein interactions and the activity of their ligands due to inducing structural rearrangements, masking or unmasking of the functional sites, and changing the ligand's intracellular localization [2]. *YWHAB*, *YWHAG*, *YWHAE*, *SFN*, *YWHAH*, *YWHAQ*, and *YWHAZ* genes encode the mammalian 14-3-3 isoforms β/α, γ, ε, σ, η, θ, and ζ/δ, respectively, where α and δ represent the phosphorylated forms. All 14-3-3 isoforms exhibit a high level of structural homology and consist of 9 antiparallel α-helices arranged in an L-shape [2,3]. Through their N-terminal region, 14-3-3 proteins form homo- and heterodimers [3]. Each ~30-kDa monomer binds to a variety of the target proteins at the consensus sequences R(S/X)XpSXP, RXXXpSXP, and pS/pTX1–2-COOH of the phosphorylated motifs [4]. The best-studied examples of the unphosphorylated targets are P*seudomonas aeruginosa* virulence factor exoenzyme S and R18, a peptide identified from a phage display library [5,6]. R18 is widely used as a potent antagonist of 14-3-3 protein/ligand interactions due to its high affinity with all 14-3-3 isoforms ($K_d$ = 80 nM) followed by occlusion of their ligand-binding groove [5]. Accordingly, dimer of R18, difopein, is also a competitive non-isoform specific inhibitor of 14-3-3 protein/ligand interactions [7].

14-3-3 proteins target a wide variety of ligands and regulate many cellular processes [2]. Accordingly, 14-3-3 proteins were shown to be involved in cardiac physiology, including cardiomyocyte development, cell cycle, and $Ca^{2+}$ signaling [8–11]. Importantly, 14-3-3 was proposed to play a role in cardiac electrophysiology due to their interactions with cardiac ion channels, exchangers, and pumps [4]. Specifically, $Na_v1.5$ was shown to coimmunoprecipitate with 14-3-3 proteins in mouse heart tissue as well as in heterologous expression systems [12]. Although 14-3-3η, -θ, and -ζ were identified by yeast 2-hybrid screen to directly interact with $Na_v1.5$, only 14-3-3η was investigated for functional consequences on the channel activity [12]. In the presence of exogenous 14-3-3η, the density of sodium current and activation curve were unchanged, while the inactivation curve was negatively shifted [12]. Based on this data, computer simulations suggested proarrhythmic effects of 14-3-3η [12]. Nevertheless, transgenic mice expressing a cardiac-specific loss-of-function 14-3-3η mutant exhibited normal cardiac morphology, cardiomyocyte appearance, and ventricular systolic function under basal conditions, while nothing was reported about its cardiac electrical activity [13]. Interestingly, immunostaining analysis revealed colocalization between exogenous 14-3-3η and $Na_v1.5$ in the intercalated discs of adult rabbit cardiomyocytes, suggesting

a role in clusterization [12]. In line with these findings, 14-3-3 proteins were reported to mediate the coupled gating of $Na_v1.5$ [14]. Although two 14-3-3 binding sites were identified in the intracellular loop between domains I and II of $Na_v1.5$ by co-immunoprecipitation analysis, it was unclear which isoform mediated the channel gating properties through its direct interaction [14]. Therefore, our goal was to investigate the direct role of all 14-3-3 isoforms on $Na_v1.5$ in a heterologous expression system. Specifically, we addressed their interaction, expression, trafficking, and sodium current.

## Materials and Methods

### *cDNA constructs and cloning*

Template cDNA constructs and their derivatives are listed in Table 1.

<table>
<tr><th>cDNA construct</th><th>Transcript (Genbank)</th><th colspan="2">Source</th></tr>
<tr><td>pcDNA3.1</td><td>Empty vector</td><td colspan="2">V86020, Invitrogen</td></tr>
<tr><td>pcDNA3.1-SCN5A-WT</td><td rowspan="7">NM_000335.5</td><td colspan="2" rowspan="3">GenScript, NJ, USA</td></tr>
<tr><td>pcDNA3.1-3X-FLAG-SCN5A-WT</td></tr>
<tr><td>pcDNA3.1-HA-SCN5A-WT</td></tr>
<tr><td>pFN217K-LgBiT(Nter)-SCN5A-WT</td><td colspan="2" rowspan="4">Cloned from pcDNA3.1-SCN5A-WT into NanoBiT® CMV Flexi BiBit ready vectors (ID# CS1603B33) according to Flexi® vector systems technical manual #TM254 from Promega (Switzerland)</td></tr>
<tr><td>pFC219K-SCN5A-WT-LgBiT(Cter)</td></tr>
<tr><td>pFN218K-SmBiT(Nter)-SCN5A-WT</td></tr>
<tr><td>pFC220K-SCN5A-WT-SmBiT(Cter)</td></tr>
<tr><td>CMV/SmBiT-CA/BlastR</td><td>NM_002730.4</td><td colspan="2" rowspan="4">NanoBiT® CMV PPI control vectors (ID# CS1603B54) from Promega (Switzerland)</td></tr>
<tr><td>CMV/LgBiT-R2A/HygR</td><td>NM_004157.4</td></tr>
<tr><td>BiBiT-RI/SmBiT-CA/LgBiT-R2A/BlastR</td><td>NM_002730.4 and NM_004157.4</td></tr>
<tr><td>CMV/HaloTag®-SmBiT</td><td>HM157289.1</td></tr>
<tr><td>pcDNA3-HA-YWHAB-WT</td><td>NM_003404.5</td><td rowspan="4">a gift from Michael Yaffe [15]</td><td>Addgene #13270</td></tr>
<tr><td>pcDNA3-HA-YWHAG-WT</td><td>NM_012479.4</td><td>Addgene #13274</td></tr>
<tr><td>pcDNA3-HA-YWHAE-WT</td><td>NM_006761.5</td><td>Addgene #13273</td></tr>
<tr><td>pcDNA3-HA-SFN-WT</td><td>NM_006142.5</td><td>Addgene #11946</td></tr>
<tr><td>pcDNA3-HA-YWHAH-WT</td><td>NM_003405.4</td><td colspan="2" rowspan="3">GenScript, NJ, USA</td></tr>
<tr><td>pcDNA3-HA-YWHAQ-WT</td><td>NM_006826.4</td></tr>
<tr><td>pcDNA3-HA-YWHAZ-WT</td><td>NM_003406.4</td></tr>
<tr><td>pcDNA3-FLAG-YWHAB-WT</td><td>NM_003404.5</td><td colspan="2" rowspan="2">a gift from Dario Diviani (University of Lausanne, Switzerland)</td></tr>
<tr><td>pcDNA3-FLAG-YWHAZ-WT</td><td>NM_003406.4</td></tr>
<tr><td>pSCM YFP-difopein</td><td>Peptide sequence: SADGAPHCVPRDLSWLD LEANMCLPGAAGLDSAD GAPHCVPRDLSWLDLEA NMCLPGAAGLE</td><td colspan="2" rowspan="2">a gift from Haian Fu (Emory University School of Medicine, GA, USA)</td></tr>
<tr><td>pSCM YFP-mutant difopein R18(D12K,E14K)</td><td>Peptide sequence: PHCVPRDLSWLKLKANM CLP</td></tr>
<tr><td>pIRES-CD8-WT</td><td>NM_001768.7</td><td colspan="2" rowspan="2">a gift from David Kass (Johns Hopkins University, MD, USA)</td></tr>
<tr><td>pIRES-CD8-WT-SCN1B-WT</td><td>NM_001768.7 and NM_001037.5</td></tr>
</table>

*Table 1. Description of cDNA constructs used in this study.*

To clone *SCN5A*-WT into NanoBiT® CMV Flexi BiBit ready vectors, SgfI and PmeI restriction sites were introduced, for which the primers were designed by the Flexi® Vector Primer Design Tool (https://ch.promega.com/techserv/tools/flexivectortool/) and purchased from Eurofins Genomics (Germany) (forward primer 5'-3': GTC GGC

GAT CGC CAT GGC AAA CTT CCT ATT ACC TCG G; reverse primer 5'-3': GCG AGT TTA AAC CAC GAT GGA CTC ACG GTC CC).

*Cell culture and transfection*

Human embryonic kidney cells tsA201 (ECACC 96121229) were cultured up to 20 passages at 37°C with 5% $CO_2$ in Dulbecco's modified Eagle's culture medium (41965, Gibco™, Thermo Fisher Scientific, USA), supplemented with 2 mM L-glutamine (G7513, Sigma), 50 U/mL penicillin-streptomycin (15140122, Gibco™) and 10% heat-inactivated fetal bovine serum (10270-106, Lot: 2440045, Gibco™). When needed, cells were split using phosphate-buffered saline (PBS, 10010-015, Gibco™) and 0.05% Trypsin-EDTA (25300-054, Gibco™). cDNA constructs were introduced into cells by transfection with LipoD293™ (SL100668, SignaGen® Laboratories). Cells were harvested 48 hours after transfection unless stated otherwise. Stable cell lines tsA201-*SCN5A*-WT and tsA201-FLAG-*SCN5A*-WT were established by polyclonal selection and were maintained in culture growth media with 200 µg/mL Zeocin™ Selection Reagent (R25005, Gibco™).

*RNA extraction, reverse transcription polymerase chain reaction, and agarose gel electrophoresis*

RNA extraction was performed on PBS-prewashed cell pellets using ReliaPrep™ RNA cell Miniprep Systems according to the manufacturer's instruction (Z6010, Promega). The concentration of extracted RNA was determined by NanoDrop™ One/One$^C$ Microvolume UV-Vis Spectrophotometer (ND-ONE-W, Thermo Fischer Scientific™). Reverse transcription (RT) was performed using a High-Capacity cDNA Reverse Transcription kit (4375222, Applied Biosystems) followed by polymerase chain reaction (PCR) with GoTaq® G2 Master Mix (M7822, Promega) on Biometra TRIO Touch Thermocycler (207072X, LabGene Scientific, Switzerland). The PCR protocol was as follows: initial denaturation at 95°C for 2 minutes, 35 cycles of denaturation at 95°C for 1 minute, annealing at 60°C for 45 seconds and elongation at 72°C for 45 seconds per kb, and a final extension of 72°C for 5 minutes. PCR products were stored at 4°C. Primers with their expected amplicon sizes are listed in Table 2.

| Target gene | Forward primer 5'-3' | Reverse primer 5'-3' | Amplicon size, bp |
|---|---|---|---|
| *GAPDH* | CCTTCATTGACCTCAACTACATGG | GGGATCTCGCTCCTGGAAGATGG | 140 |
| *PSMB4* | GCACTTTACAGAGGTCCAATCAC | CTCGGTAGTACAGCACTCGC | 565 |
| *TBP* | CTTGACCTAAAGACCATTGCACTTC | GAAACTTCACATCACAGCTCCC | 266 |
| *YWHAB* | CTGCTCTCTGTTGCCTACAAGAATGT | CTTCGTCTCCCTGGTTTTCCGAT | 583 |
| *YWHAG* | GCGAGCAACTGGTGCAGAAAGC | GTACTGGGTCTCGCTGCAATTCTT | 341 |
| *YWHAE* | GACAAGCTAAAAATGATTCGGGAATATCG | CTGAAGTCCATAGTGTCAGATTATCACG | 472 |
| *SFN* | GAGAGAGCCAGTCTGATCCAGAA | GTAGTAGTCACCCTTCATCTTCAGGTAG | 381 |
| *YWHAH* | TACGACGACATGGCCTCCG | CAAACTGTCTCCAGCTCCTTCTCA | 233 |
| *YWHAQ* | GCTCTCCGTGGCCTACAAGAAC | CGATCATCACCACACGCAACTTCA | 285 |
| *YWHAZ* | GATGACAAGAAAGGGATTGTCGATCAGT | CACTTAATGTATCAAGTTCAGCAATGGCT | 217 |

*Table 2. Description of primers used in this study.*

*Protein lysate extraction*

Pre-washed (PBS) adherent monolayers of cells were scraped in 2 mL of cold PBS (pH 7,4) and pelleted by centrifugation for 5 minutes at 200 g at 4°C. Cell pellets were lysed in lysis buffer (50 mM NaCl, 50 mM imidazole/HCl, 2 mM 6-aminohexanoic acid,

1 mM EDTA, pH 7) with addition of cOmplete tablets EDTA-free (04693132001, Roche, Switzerland), 0.5 mM $Na_3VO_4$, 0.5 mM NaFl, 10 µg/ml aprotinin, 10 µg/mL leupeptin, 1 mM phenylmethylsulfonyl fluoride and 1% digitonin (D141, Sigma) for 1 hour at 4°C. Lysates were centrifuged at 16,100 g for 15 minutes at 4°C. The obtained supernatant was taken for further analysis. Protein concentration was determined by Coo Assay Protein Dosage Reagent (Uptima, UPF86420).

*Co-immunoprecipitation*

To immunoprecipitate FLAG-tagged proteins, anti-FLAG® M2 Magnetic Beads (M8823, Sigma) were used in the proportion of 1 µL of beads per 10 µg of total protein lysate. Protein lysates were diluted in Tris-buffered saline (TBS, 20 M Tris, 0.1 mM NaCl, pH 7.6 (HCl-adjusted)) and were mixed with the TBS-prewashed beads at 4°C overnight. After thoroughly washing the beads with TBS, the FLAG-specific co-immunoprecipitated protein complex was eluted with 4X LDS sample buffer (NP0007, Invitrogen). The samples were analyzed with the immunoblotting technique (see below).

*Cell surface biotinylation assay*

Adherent cell monolayers were gently washed three times with cold PBS (pH 8) and incubated, while slowly rocking, with 1 mg/mL EZlink™ Sulfo-NHS-SS-Biotin (21331, Thermo Fisher Scientific) in PBS (pH 8) for 45 minutes at 4°C. Afterward, the excess biotin was quenched by washing with 50 mM Tris-HCl (pH 8), followed by several washes with PBS (pH 7,4). Extracted protein lysates were mixed with Streptavidin Sepharose High-Performance beads (GE Healthcare, USA) at 4°C overnight. After thoroughly washing the beads with washing buffer (0.1% BSA, 0.001% Tween20, PBS pH 7,4), the biotinylated fraction was eluted with 4X LDS sample buffer and analyzed with the immunoblotting technique (see below).

*Sodium dodecyl sulfate–polyacrylamide gel electrophoresis (SDS-PAGE) and immunoblotting analysis*

Protein lysates containing LDS sample buffer and 100 mM dithiothreitol (DTT) were loaded onto 4-12% Tris-acetate acrylamide gels and let to run at 60 mV in Tris-acetate running buffer (50 mM Tris, 50 mM Tricine, 0.1% SDS, pH 8.3). Afterward, proteins were transferred to the nitrocellulose membrane by using the Trans-Blot Turbo system (1704158, Bio-Rad, USA). After validation of successful protein transfer with Ponceau S solution (0.1% Ponceau S, 12.5% acetic acid), the membranes were blocked with 5% bovine serum albumin (BSA) in TBS-T (TBS, 0.1% Tween20) for 1 hour at room temperature and then incubated with primary antibody dilutions at 4°C overnight. After incubating membranes with secondary antibodies for 1 hour at room temperature, the infrared fluorescent signals were revealed with LiCor Odyssey Infrared imaging system (LI-COR Biosciences) and quantified with ImageJ software (Rasband, W.S., U. S. National Institutes of Health, Bethesda, Maryland, USA).

Primary and secondary antibodies used in this study are listed in Table 3.

| Target protein | Dilution | Host | Source |
|---|---|---|---|
| FLAG | 1:1000 | mouse | F1804, Sigma |
| GFP | 1:1000 | mouse | 1814460001, Roche (Switzerland) |

| GFP | 1:1000 | rabbit | AB514, Eurogen |
|---|---|---|---|
| HA | 1:500 | mouse | ENZ-ABS118-0500, Enzo Life Sciences |
| HA | 1:1000 | rabbit | ab137838, Abcam (UK) |
| $Na_v1.5$ | 1:1000 | rabbit | generated by Pineda (Germany) |
| α1-$Na^+$/$K^+$ ATPase | 1:500 | mouse | ab7671, Abcam (UK) |
| α1-syntrophin | 1:1000 | rabbit | generated by Pineda (Germany) |
| α-actin | 1:1000 | rabbit | A-2066, Sigma |
| IRDye$^R$ 680RD anti-mouse red | 1:20,000 | goat | 926-68070, LI-COR Biosciences |
| IRDye$^R$ 800CW anti-rabbit green | 1:20,000 | goat | 926-32211, LI-COR Biosciences |

*Table 3. Description of primary and secondary antibodies used in this study.*

*Patch clamp electrophysiology*

To test data replicability, whole-cell sodium current recordings from two researchers using different setups were pooled together: either with an Axopatch 200B amplifier (Molecular Devices, Wokingham, United Kingdom) or with a VE-2 amplifier (Alembic Instrument, USA). Cells, solutions, micropipettes, and protocols were identical.

All cells were transiently co-transfected with *CD8*. Only successfully transfected cells, visualized by brief pre-wash with 1:1000 dilution of Dynabeads™CD8 (Thermo Fisher Scientific), were chosen for electrophysiological recordings. Thin-wall capillaries (TW150F-3, World Precision Instruments, Germany) were pulled with a DMZ-universal puller (Zeitz, Germany) with a tip resistance of 1.0 to 3.0 MΩ. The intracellular pipette solution contained (in mM): $Na_2ATP$ 5, CsAsp 70, CsCl 60, EGTA 11, $CaCl_2$ 1, $MgCl_2$ 1, HEPES 10. The extracellular solution contained (in mM): NaCl 20, NMDG-Cl 110, $CaCl_2$ 2, $MgCl_2$ 1.2, HEPES 10, CsCl 5, D-glucose 5. pH was adjusted to 7.2-7.4 with CsOH or HCl. Osmolarity was measured by Osmometer type OM 806 (Löser). All recordings were performed at a stable temperature of 25°C using Axon™ pCLAMP™ 10 Electrophysiology Data Acquisition & Analysis Software, Version 10.2 (Axon Instruments, CA, USA). The recorded sodium current $I_{Na}$ was filtered at 5 kHz at a sampling rate of 20 kHz per signal. Recordings without leak subtraction were selected for analysis. Raw traces were not corrected for the liquid junction potential.

Exclusion criteria for individual traces were: absence of $I_{Na}$; current at holding potential (-100 mV) <= -100 pA; slope of the steady-state activation (SSA) curve <=4; and slope of the steady-state inactivation (SSI) curve >=8. Sodium current density (pA/pF) was calculated by dividing peak current by cell capacitance. Current-voltage (I–V) curves were fitted with the equation $y = g(V_m - V_{rev})/((1 + \exp[(V_m - V_{1/2})/k]))$. SSI and SSA curves were fitted with the Boltzmann equation $y = 1/(1 + \exp[(V_m - V_{1/2})/k])$, where $y$ is the normalized current or conductance at a given holding potential, $V_m$ is the membrane potential, $V_{rev}$ is the reversal potential, $V_{1/2}$ is the potential at which half of the channels are activated, and $k$ is the slope factor.

*Protein-protein interaction assay*

The NanoLuc® Binary Technology, NanoBiT® (Promega) allowed us to monitor protein-protein interactions between two $Na_v1.5$-WT subunits in live cells using an aqueous, cell-permeable furimazine substrate. For this purpose, *SCN5A*-WT was cloned into different vectors that encoded $Na_v1.5$-WT tagged with Large BiT (LgBiT)

and Small BiT (SmBiT) on N- or C-termini when transfected into tsA201 cells. In the case of physical interaction between LgBiT and SmBiT, the bright luminescent signal was formed. Since Nano-Glo® Live Cell Assay (N2012, Promega) was not ratiometric and depended on the cell quantity, we normalized the luminescent signal to the fluorescent signal obtained with CellTiter-Fluor® Cell Viability assay (G6082, Promega). The signals were detected with Spark® multimode microplate (Tecan).

*Data and statistical analysis*

Data are represented as means ± SEM and are compared to the wild-type condition unless indicated otherwise. Statistical significance was calculated with a two-tailed Mann–Whitney U-test, or by two-way ANOVA and Tukey's multiple comparisons test when comparing more than two groups (Prism version 7.04; GraphPad, CA, USA). We considered a $p$-value < 0.05 to indicate a statistically significant difference.

## Results

*Identification of 14-3-3 isoforms interacting with $Na_v1.5$*

To identify which 14-3-3 isoform interacts with Nav1.5, we performed co-immunoprecipitation analysis. Individual overexpression of all seven human 14-3-3 isoforms tagged with HA revealed that by themselves 14-3-3 proteins have a certain degree of non-specific binding with the anti-FLAG magnetic beads (Suppl. fig. S1-4). Accordingly, the control condition with non-tagged $Na_v1.5$ was run along with FLAG-$Na_v1.5$ and compared for the intensity of co-immunoprecipitated 14-3-3 protein. As an indicator of successfully co-immunoprecipitated $Na_v1$-5-specific fraction, we used α1-syntrophin, a known partner of $Na_v1.5$ macromolecular complex and endogenously present in tsA201 [16]. From all the isoforms, only 14-3-3η exhibited a stronger band intensity in the FLAG-immunoprecipitated fraction compared to the non-tagged fraction; hence, we concluded that only this isoform reliably interacts with $Na_v1.5$ (Fig. 1). Since no differences were detected between transient and stable overexpression of *SCN5A*, further experiments were mainly performed on tsA201 stably expressing $Na_v1.5$ (Suppl. fig. S1-4).

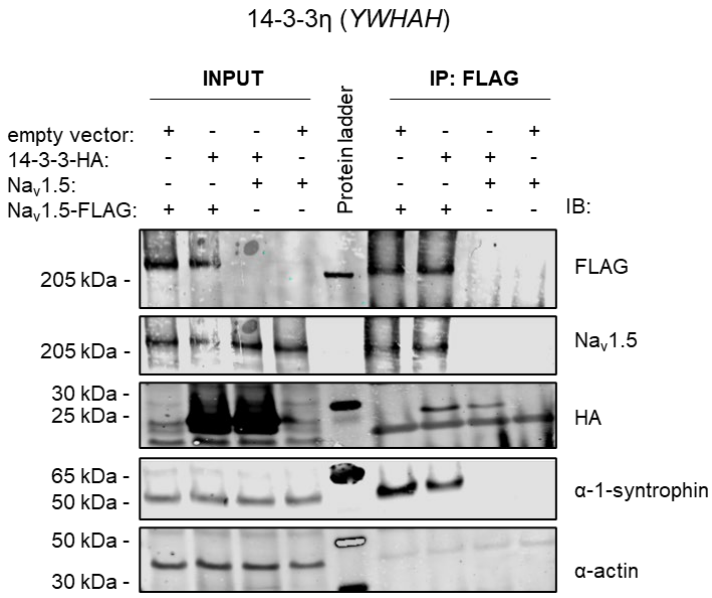


**Figure 1. Co-immunoprecipitation between $Na_v1.5$ and 14-3-3η.** Representative immunoblot of total lysate and FLAG-specific immunoprecipitated fraction of tsA201 cells 48 hours after transient transfection with *YWHAH* and *SCN5A*. Overexpressed HA-tagged 14-3-3η was revealed with an anti-HA antibody. Endogenous α1-syntrophin was used as a positive control for co-immunoprecipitation with $Na_v1.5$, and α-actin as a negative control.

*14-3-3 proteins do not affect expression level of $Na_v1.5$ at the cell surface*

Next, we assessed the role of 14-3-3 proteins on the cell surface density of $Na_v1.5$. This was motivated by findings from Pohl *et al.*, who suggested that 14-3-3 proteins modulate cell surface expression of membrane receptors and ion channels upon binding with the E3 ubiquitin ligase Nedd4-2 [17]. Specifically, they showed that the high affinity of 14-3-3 with phosphorylated Ser342 and Ser448 sites of Nedd4-2 induces its structural rearrangement with plausible exposure of its tryptophan-rich (WW) domain [17]. Our group previously reported the interaction between the WW domain of Nedd4-2 with the PY-motif of $Na_v1.5$ and its importance for $Na_v1.5$ cell surface localization [18,19]. According to our current results, the levels of the total and cell surface $Na_v1.5$ expression, represented by the biotinylated fraction, did not change upon overexpression of each individual 14-3-3 isoform when compared to the sodium channel alone (Fig. 2A).

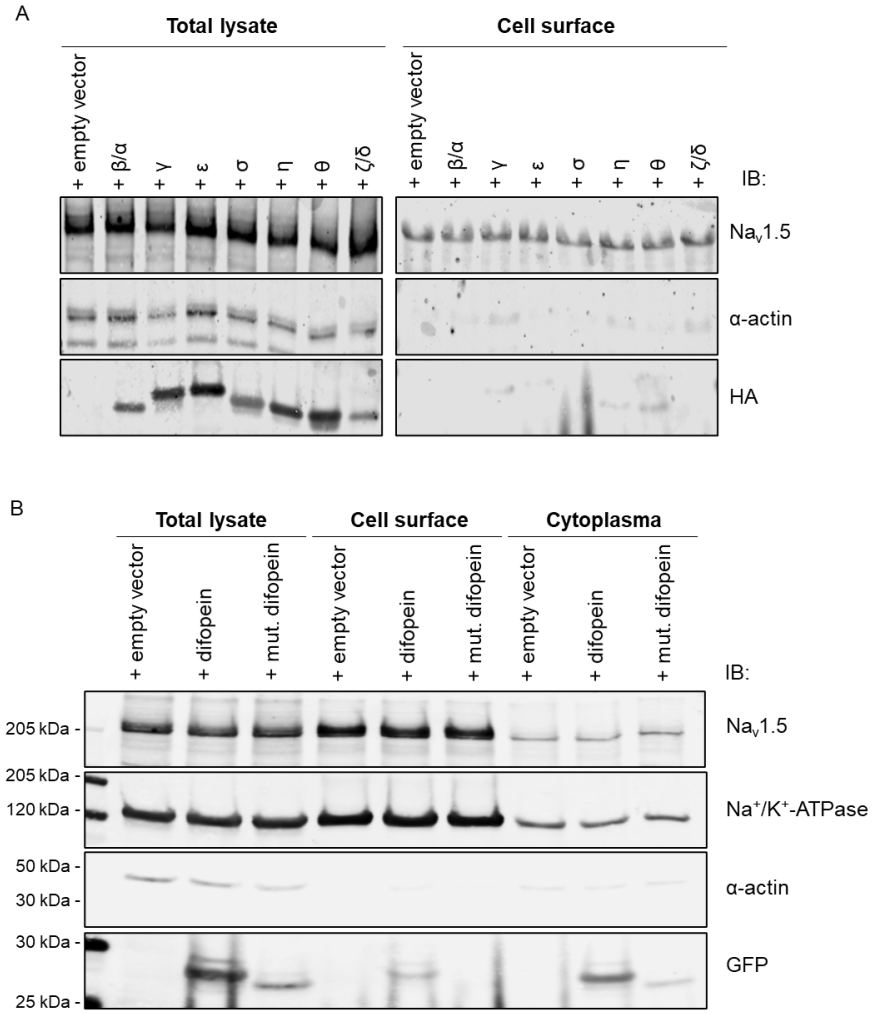


**Figure 2. 14-3-3 proteins do not affect the total expression level of $Na_v1.5$ and cell surface density.** Representative immunoblot of the total lysate and biotinylated fraction of tsA201 stably expressing $Na_v1.5$ after 48 hours of transient overexpression of: A, 14-3-3 proteins tagged with HA; B, difopein and mutant of difopein. Overexpressed HA-tagged 14-3-3 proteins were revealed with anti-HA antibody. Endogenous $Na^+/K^+$-ATPase was used as a positive control of cell surface fraction, while α-actin was used as a negative control. Overexpressed YFP-tagged difopein and its mutant were revealed with an anti-GFP antibody.

Of note, in tsA201, we detected endogenous mRNAs of all 14-3-3 isoforms (Suppl. fig. S5). In line with our results, transcripts of all 14-3-3 isoforms were previously reported for HEK293, the cell line from which tsA201 was originally derived [20]. Therefore, to inhibit endogenous 14-3-3/ligand interactions, we used difopein, a dimer of R18, the unphosphorylated peptide antagonist of 14-3-3 [7]. Difopein strongly interacts with two 14-3-3 proteins, stabilizing them in dimeric conformation, occupying their binding grooves, and preventing their interaction with other ligands [7]. We performed co-immunoprecipitation analysis to validate that difopein is an effective competitor for 14-3-3/ligand interactions in our heterologous expression system. First, we confirmed that 14-3-3 strongly interacts with difopein but not with its mutant (Suppl. fig. S6A). As expected, difopein-YFP exhibited higher molecular weight than the mutant difopein-YFP, represented by the monomeric R18-D12K,E14K peptide (Suppl. fig. S6A). Further, we demonstrated that 14-3-3 dimers were stabilized by difopein but not by its mutant (Suppl. fig. S6B). Last, we confirmed that such an effect did not depend on any specific 14-3-3 isoform (Suppl. fig. S6B). Of note, difopein and its mutant did not affect the total and cell surface expression of $Na_v1.5$ (Fig. 2B). Therefore, we concluded that 14-3-3 proteins do not regulate $Na_v1.5$ expression and cell surface density in the tested heterologous expression system.

*Impact of 14-3-3 proteins onto $Na_v1.5$-mediated sodium current*

Since of all 14-3-3 isoforms, only 14-3-3η directly interacted with $Na_v1.5$ (Fig. 1), we assessed the whole cell recordings of the sodium current ($I_{Na}$) when transiently overexpressing *YWHAH*, encoding 14-3-3η. Moreover, to establish comparable conditions with the previous study that described a 14-3-3η-induced negative shift in $I_{Na}$ inactivation curve, we similarly co-expressed *SCN1B*, encoding the $Na_v\beta1$ subunit of the voltage-gated sodium channel [12]. In our heterologous expression system, neither 14-3-3η or Navβ1 alone nor their combination modified the baseline whole-cell properties of $I_{Na}$, as described by the current-voltage (*I-V*) relationship, peak current density, reversal potential ($V_{rev}$) and half-maximal potentials ($V_{1/2}$) of activation and inactivation curves (Fig. 3, Table 4). However, when difopein disrupted endogenous 14-3-3/ligand interactions, $Na_v1.5$ currents were considerably upregulated with a slight and significant shift of the activation curve towards more negative potentials (Fig. 4, Table 5). In summary, the isoform non-specific antagonist of 14-3-3 difopein positively regulated $Na_v1.5$-mediated currents, whereas 14-3-3η, the only isoform interacting with $Na_v1.5$, left the channel function unmodified.

| | | | **Steady-state activation** | | **Steady-state inactivation** | |
|---|---|---|---|---|---|---|
| | Peak $I_{Na}$ density (pA/pF) | $V_{rev}$ (mV) | *k* slope | $V_{1/2}$ (mV) | *k* slope | $V_{1/2}$ (mV) |
| **+ CD8 + empty vector (n=32, N=11)** | -140.18 ± 14.11 | 38.15 ± 1.68 | 6.38 ± 0.17 | -27.01 ± 0.89 | 5.25 ± 0.12 | -78.93 ± 0.90 |
| **+ CD8 + 14-3-3η (n=32, N=11)** | -120.69 ± 19.06 | 35.62 ± 1.13 | 6.45 ± 0.18 | -26.02 ± 1.38 | 5.22 ± 0.16 | -78.98 ± 0.97 |
| **+ CD8 + $hNa_v\beta1$ + empty vector (n=31, N=10)** | -129.51 ± 17.83 | 35.59 ± 1.35 | 6.49 ± 0.13 | -27.61 ± 1.22 | 4.97 ± 0.14 | -79.86 ± 1.10 |
| **+ CD8 + $hNa_v\beta1$ + 14-3-3η (n=28, N=9)** | -143.15 ± 16.60 | 36.88 ± 1.57 | 6.39 ± 0.17 | -25.05 ± 1.18 | 5.35 ± 0.17 | -77.75 ± 0.90 |

*Table 4. Biophysical properties of sodium currents conducted by $Na_v1.5$ stably present in tsA201 cells in combination with transiently expressed 14-3-3η and/or $Na_v\beta1$. CD8 was co-expressed to visualize successfully transfected cells. Peak sodium current ($I_{Na}$) densities are extracted from the respective I-V curves. Data are presented as mean ± SEM and are compared to control values (i.e., "+CD8 + empty vector"). n, number of cells analyzed; N, number of biological replicates.*

| | | | Steady-state activation | | Steady-state inactivation | |
|---|---|---|---|---|---|---|
| | Peak $I_{Na}$ density (pA/pF) | $V_{rev}$ (mV) | *k* slope | $V_{1/2}$ (mV) | *k* slope | $V_{1/2}$ (mV) |
| **+ CD8 + empty vector (n=40, N=12)** | -127.62 ± 12.46 | 48.94 ± 2.74 | 6.18 ± 0.14 | -26.39 ± 1.05 | 5.15 ± 0.11 | -77.43 ± 0.92 |
| **+ CD8 + difopein (n=34, N=12)** | -191.06 ± 19.84 ** | 47.73 ± 2.50 | 6.04 ± 0.19 | -28.66 ± 1.00 | 5.09 ± 0.13 | -78.22 ± 0.83 |
| **+ CD8 + mut. difopein (n=42, N=10)** | -124.05 ± 14.62 | 42.62 ± 2.30 | 6.47 ± 0.14 | -26.85 ± 1.07 | 5.10 ± 0.11 | -78.95 ± 0.94 |

*Table 5. Biophysical properties of sodium currents conducted by $Na_v1.5$ stably present in tsA201 cells in combination with transiently expressed difopein and its mutant. CD8 was co-expressed to visualize successfully transfected cells. Peak sodium current ($I_{Na}$) densities are extracted from the respective I-V curves. Data are presented as mean ± SEM and are compared to control values (i.e., "+CD8 + empty vector"). **, $p < 0.01$. n, number of cells analyzed; N, number of biological replicates.*

*Inhibition of 14-3-3 dimerization does not affect the interaction between α-subunits of $Na_v1.5$.*

One role of the 14-3-3 family of adapter proteins is to stabilize multiprotein complexes [2]. In particular, 14-3-3η was proposed to mediate the coupled gating of $Na_v1.5$ dimers by bridging two α-subunits through their DI-DII loops [14]. However, since overexpressed 14-3-3 isoforms did not promote $Na_v1.5$ dimerization (Fig. 1, Suppl. fig. S1-4), we evaluated whether the 14-3-3 antagonist difopein affected $Na_v1.5$ dimerization. Our co-immunoprecipitation analysis confirmed the existence of $Na_v1.5$-$Na_v1.5$ interactions in a heterologous expression system, but these were not affected by difopein alone or by difopein with 14-3-3η overexpression (Fig. 5A-B, Suppl. fig. S7A). To confirm this finding in a more physiological and dynamic environment, we performed a NanoBiT assay. In brief, N- and C-termini of $Na_v1.5$ were tagged with LgBiT and SmBiT, respectively, which are parts of the bright and stable Nanoluciferase. Accordingly, when two $Na_v1.5$ physically interact, LgBiT and SmBiT would reconstitute Nanoluciferase, subsequently leading to luminescence emission (Fig. 5C). In live tsA201 cells, the level of interaction between two $Na_v1.5$ was not modified by difopein alone or by difopein with overexpressed 14-3-3η (Fig. 5D-G, Suppl. fig. S7B-E). Interestingly, when comparing various locations of LgBiT and SmBiT tags on $Na_v1.5$, the brightest luminescent signal was detected when N-N and C-C termini were combined, compared to the N-C and C-N conditions (Fig. 5D-G). It might indicate a preferred conformational orientation of α-subunits within $Na_v1.5$ dimers.

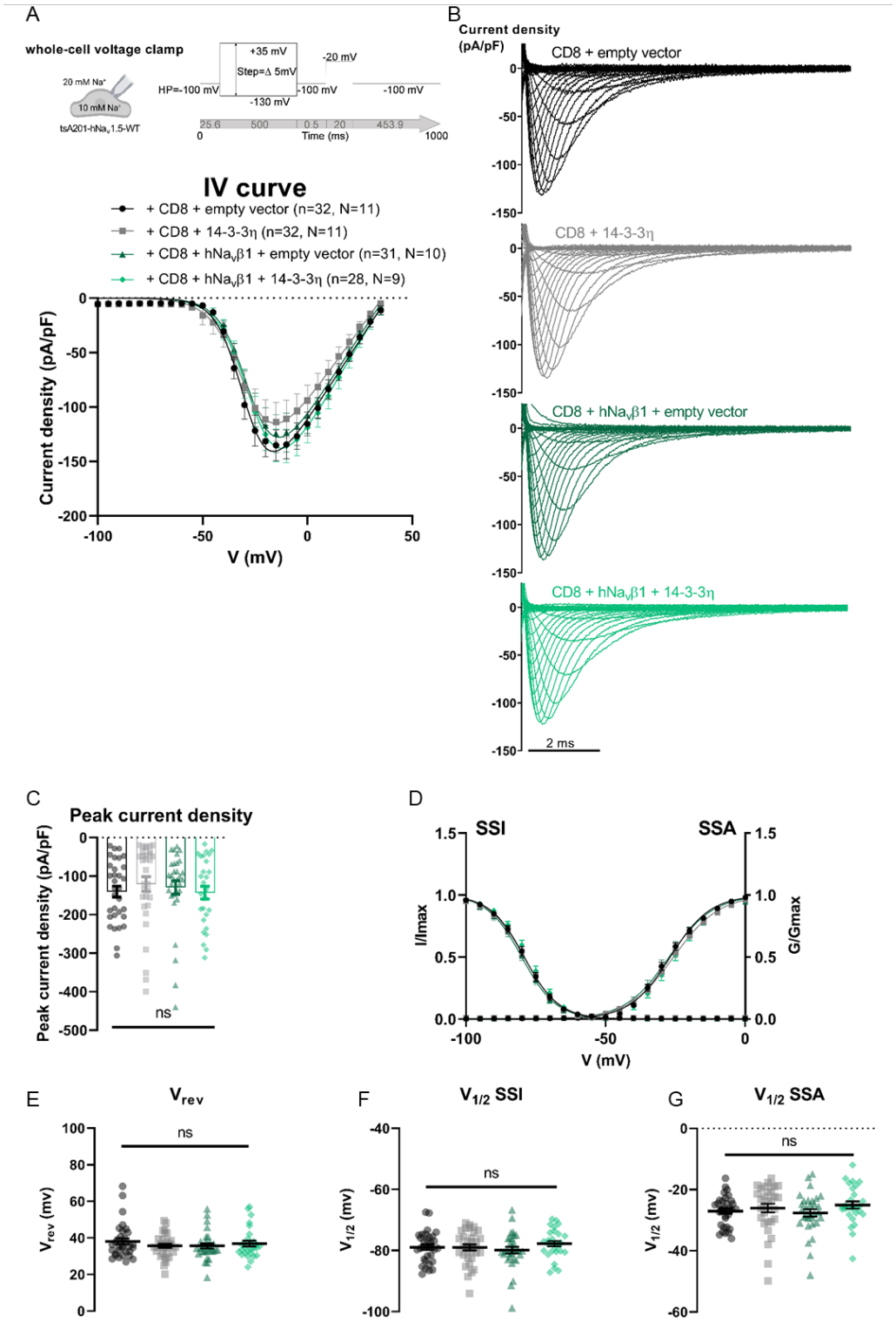


**Figure 3. 14-3-3η expressed alone or with $Na_v\beta1$ does not affect $Na_v1.5$-conducted sodium current.** A, Current density-voltage (IV) relationships from tsA201-$Na_v1.5$ transiently expressing CD8 with empty vector, or 14-3-3η, and/or $Na_v\beta1$. B, Representative whole-cell $I_{Na}$ traces recorded from the listed conditions. C, Peak current densities of each group. D, Steady-state activation (SSA) and steady-state inactivation (SSI) curves. E, Reversal potential ($V_{rev}$). F, Half-voltage of SSI ($V_{1/2}$ SSI). G, Half-voltage of SSA ($V_{1/2}$ SSA). Values pertaining to the biophysical properties are shown in Table 4. Data are presented as mean ± SEM. *n*, number of cells taken for analysis; *N*, number of biological replicates. ns, non-significant.

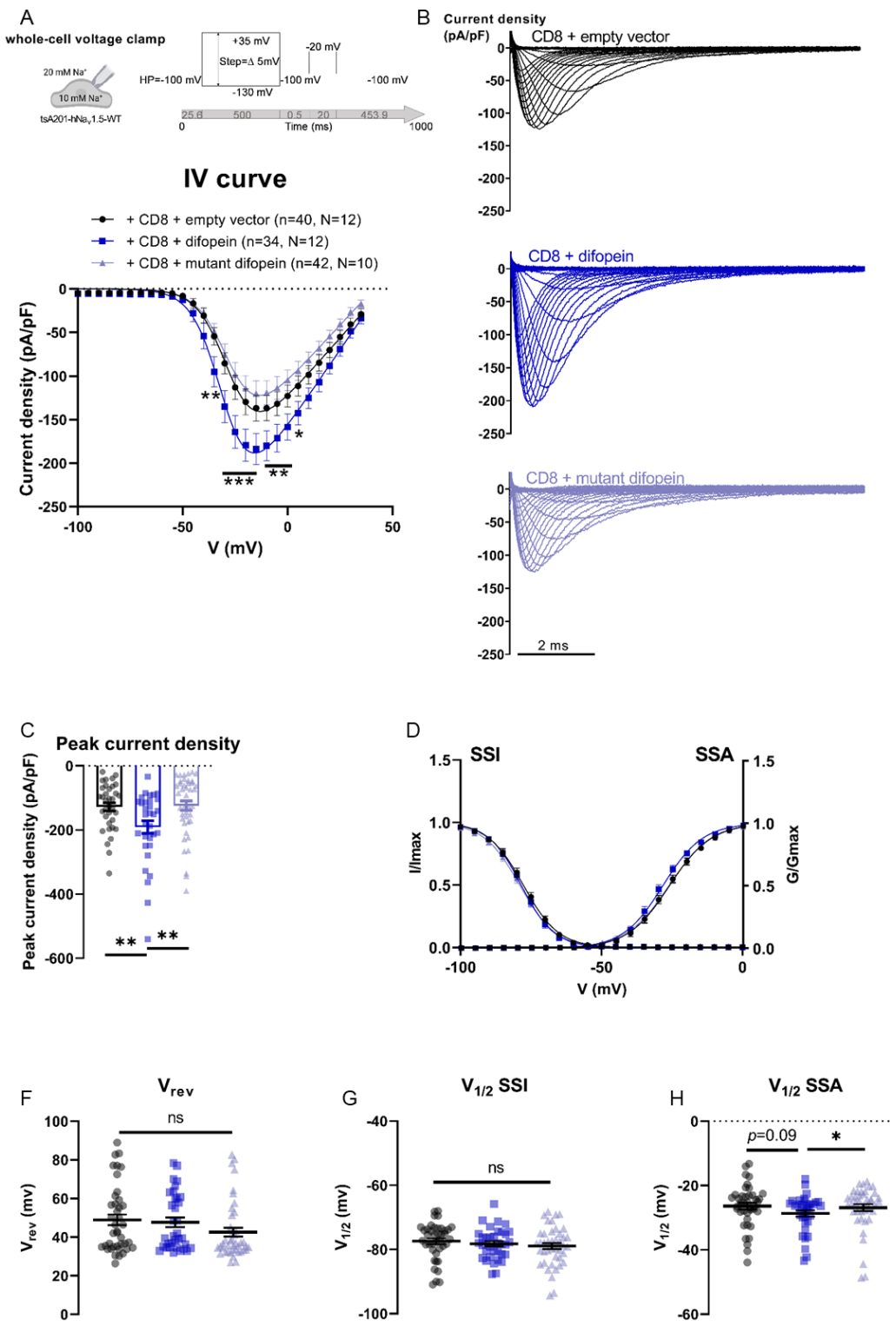


**Figure 4. Difopein, an antagonist of 14-3-3/ligand interactions, upregulates $Na_v1.5$-mediated sodium current.** A, Current density-voltage (IV) relationships from $Na_v1.5$-expressing tsA201 cells transiently expressing CD8 with empty vector, difopein, or mutant of difopein. B, Representative whole-cell $I_{Na}$ traces recorded from the listed conditions. C, Peak current densities of each group. D, Steady-state activation (SSA) and steady-state inactivation (SSI) curves. E, Reversal potential ($V_{rev}$). F, Half-voltage of SSI ($V_{1/2}$ SSI). G, Half-voltage of SSA ($V_{1/2}$ SSA). Values pertaining to the biophysical properties are shown in Table 5. Data are presented as mean ± SEM. *n*, number of cells taken for analysis; *N*, number of biological replicates. ns, non-significant; *, $p < 0.05$; **, $p < 0.01$; ***, $p < 0.001$.

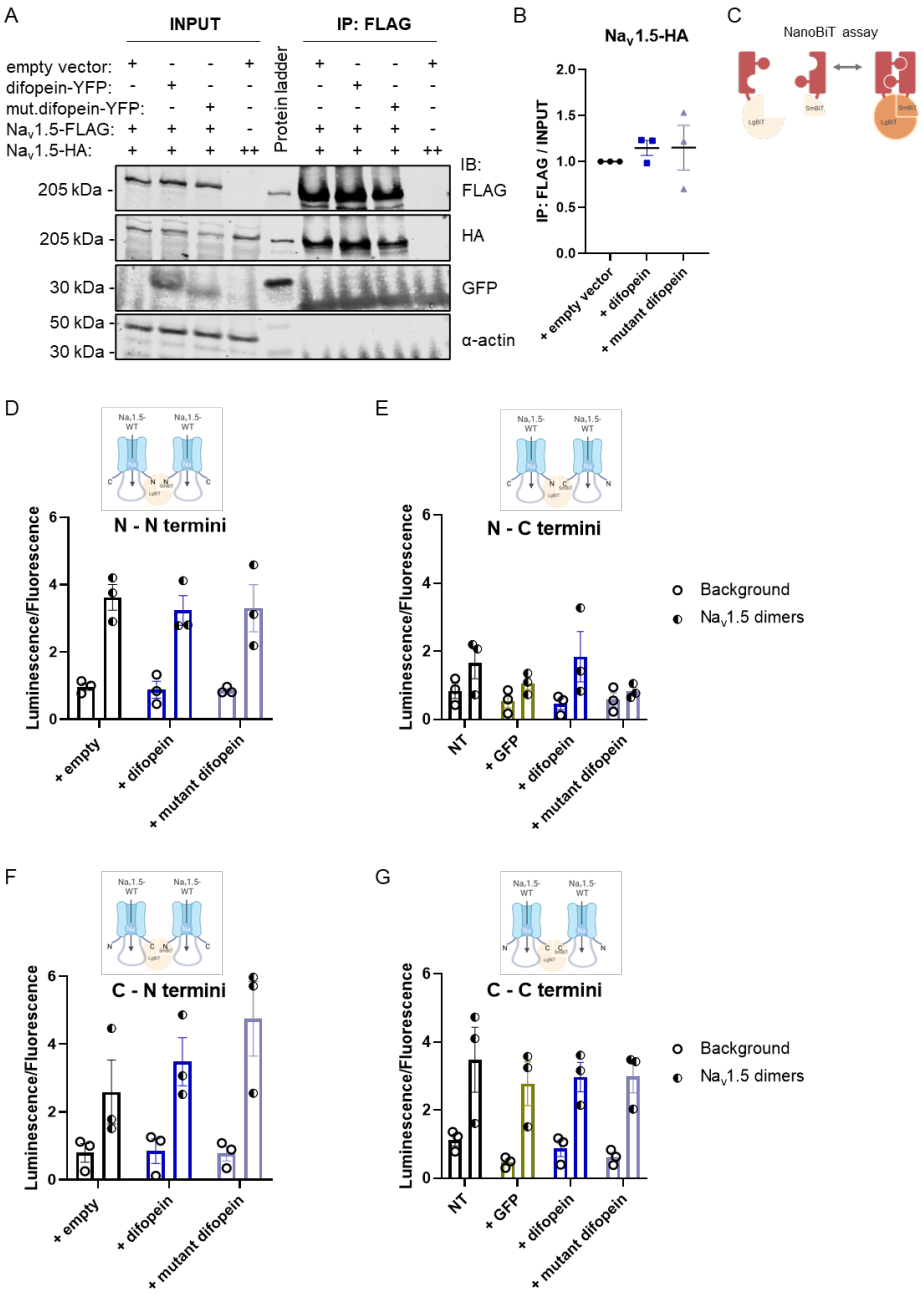


**Figure 5. Inhibition of 14-3-3/ligand interaction does not affect oligomerization between α-subunits of $Na_v1.5$.** A, difopein and its mutant did not affect co-immunoprecipitation between α subunits of $Na_v1.5$. B, representative immunoblot of the total lysate ("input") and FLAG-specific immunoprecipitated fraction ("IP: FLAG") of tsA201 cells transiently expressing $Na_v1.5$ with empty vector, difopein, or mutant of difopein. Overexpressed YFP-tagged difopein and its mutant were revealed with an anti-GFP antibody. Endogenous α-actin was used as a negative control for co-immunoprecipitation with $Na_v1.5$. The relative intensity of co-immunoprecipitated $Na_v1.5$-HA was normalized to the intensity of the total $Na_v1.5$-HA and normalized to the control condition ("+empty vector"). Data presented as mean ± SEM from three biological replicates. C, schematic illustration of NanoBiT assay. D,E,F,G, in living cells, difopein did not modify the level of $Na_v1.5$ dimers. Results of the NanoBiT assay are presented as relative intensity of luminescence (indicating the level of protein-protein interactions) normalized to fluorescence (indicating the number of cells) in tsA201 cells transiently transfected with *SCN5A* constructs. Different variations between $Na_v1.5$ N- and C-termini interactions were tested. Background signal was determined by co-expression of N- or C-termini LgBiT-$Na_v1.5$ with non-interacting control (SmBiT-HaloTag). Since difopein and its mutant were tagged with YFP, we also included control by co-transfection with GFP. NT, non-transfected.

## Discussion

We reported that amongst seven 14-3-3 isoforms, only η (encoded by *YWHAH*) co-immunoprecipitated with the major cardiac voltage-gated sodium channel $Na_v1.5$ when heterologously expressed in tsA201 cells. Nevertheless, neither 14-3-3η overexpression nor its inhibition with difopein affected the total protein level of $Na_v1.5$, its cell surface localization, or dimerization. Interestingly, while 14-3-3η did not modify the basal biophysical properties of $I_{Na}$, difopein induced functional upregulation of $Na_v1.5$.

Our finding that 14-3-3 interacts with Nav1.5, and 14-3-3η expression does not affect $I_{Na}$ density (Fig. 1 and Fig. 3) are in line with several previous reports. Allouis et al., for instance, have demonstrated previously that 14-3-3 interacted with $Na_v1.5$ in COS-7 cells and native mouse cardiac tissue, and endogenous and exogenous 14-3-3η did not modify $I_{Na}$ density and activation parameters of $Na_v1.5$ [12]. Similarly, another study showed that inhibition of endogenous 14-3-3η did not alter $I_{Na}$ density in CHO cells [21]. Our observation that 14-3-3 proteins do not participate in the dimerization of heterologously expressed $Na_v1.5$ was also corroborated by previous reports [14,21]. Both studies highlighted that instead of directly mediating the formation of $Na_v1.5$ homo- and heterocomplexes with other ion channels (*e.g.*, $Na_v1.5$-$Na_v1.5$ and $Na_v1.5$-$K_{ir2.1}$), 14-3-3η played a significant role in their biophysical coupling [14,21].

However, our finding that 14-3-3 did not alter $I_{Na}$ biophysical properties conflicts with previous reports. Allouis *et al.* showed that 14-3-3η shifted the inactivation curve to more negative potentials and decelerated the recovery from the inactivation of $Na_v1.5$ [12]. By co-expressing *SCN1B*, we eliminated the possibility that such discrepancy could be due to the presence of the $Na_v\beta1$ subunit. Unlike the tsA201 cells used in our study, Allouis *et al*. used Cos-7 cells derived from monkey kidney fibroblasts as their heterologous expression system [12]. Like tsA201 cells, Cos-7 endogenously express all seven 14-3-3 isoforms, too [22]. However, their expression pattern, representing subcellular localization of 14-3-3 proteins, differed noticeably from human embryonic kidney (HEK293) cells [22]. Furthermore, other protein partners that regulate the function of $Na_v1.5$ may also vary between cellular models and may explain the disparity of our outcomes.

Having identified 14-3-3η as the only isoform directly interacting with $Na_v1.5$ but not affecting $I_{Na}$, we did not expect the 14-3-3 antagonist difopein to modulate the $I_{Na}$ so significantly (Fig. 4). Our finding is especially surprising since Clatot *et al*. did not report any difopein-induced increase of $I_{Na}$ in HEK293 cells [14]. Since $Na_v1.5$ is regulated by many proteins, including kinases, of which many are 14-3-3 substrates, too [23,24], it is plausible that difopein could alter the function of $Na_v1.5$ indirectly through other partner proteins (Fig. 6). Indeed, monomeric peptide R18, of which difopein is composed, disrupts 14-3-3γ/ε from protein kinase A (PKA), unmasking PKA's catalytic activity and promoting PKA-mediated phosphorylation of its downstream targets [25]. $Na_v1.5$ is among PKA's targets, and PKA stimulation in HEK293 cells has been shown to enhance $I_{Na}$ [26]. Furthermore, 14-3-3γ was shown to slow dephosphorylation of calcium/calmodulin-dependent protein kinase (CaMKII) [27]. CaMKII is reported to mediate both gain- and loss-of-function effects of $I_{Na}$, highlighting its complex

relationship with $Na_v1.5$ [23]. Moreover, 14-3-3ζ has been shown to regulate protein kinase C (PKC), which, in turn, also modulates $Na_v1.5$ activity through phosphorylation [28]. Our finding of difopein-induced $I_{Na}$ increase might therefore be attributed to the inhibition of several 14-3-3 isoforms, affecting the phosphorylation-dependent gating of $Na_v1.5$ (Fig. 6).

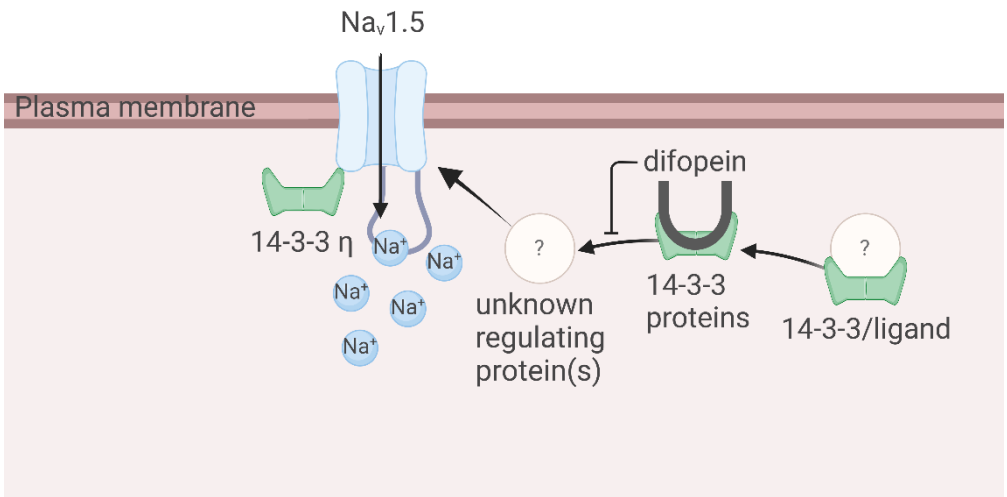


**Figure 6. Working model of the indirect effect of 14-3-3 proteins on the $Na_v1.5$ channel.** In the tested heterologous expression system, 14-3-3η is the only isoform directly interacting with $Na_v1.5$ without affecting the whole-cell current density of $I_{Na}$. Surprisingly, whole-cell current density was increased in presence of difopein, an antagonist of 14-3-3/ligand interactions. We suggest that this effect is due to difopein inhibiting 14-3-3 interactions with other tsA201-endogenous proteins that may regulate $Na_v1.5$.

*Limitations*

To eliminate possible clonal specificity of our cell model, we developed polyclonal tsA201 stably expressing $Na_v1.5$. This led to high variability in whole-cell $Na_v1.5$ expression, which made single-cell electrophysiological analyses challenging, we strengthened the reliability of our data by testing a relatively large number of cells for each condition.

Since 14-3-3 isoforms not only homodimerize but also form heterodimers, the presence of all endogenous isoforms in our cell model could be a limitation of this study. In our case, overexpressed 14-3-3η heterodimerizing with other isoforms could interact with substrates other than $Na_v1.5$, hindering its direct role on the channel. Therefore, using gene-editing techniques to silence specific isoforms would be advantageous to unravel the complexity of 14-3-3 signaling.

Another limitation of heterologously expressed proteins is the difficulty in controlling post-translational modifications, such as phosphorylation, that impact $Na_v1.5$ function and 14-3-3 signaling. A recent study reported a successful semisynthetic approach to stabilize $Na_v1.5$ phosphorylation *in vitro* [29]. Thus, it would be interesting to test difopein-mediated regulation under stably phosphorylated $Na_v1.5$.

While 14-3-3 might not act directly onto $Na_v1.5$, it was shown to act onto its macromolecular complex with other protein partners (*e.g.*, PKA, PKC, CaMKII) and cardiac ion channels (*e.g.*, Kir2.1) [17,21]. Because of the vast spectrum of 14-3-3 targets,

one should be aware of the possible indirect effects measured in any experiment targeting 14-3-3 function. As such, any results obtained with difopein should be interpreted carefully.

In summary, while direct effects of 14-3-3, specifically isoform η, on the cardiac sodium channel are not evident in the tested heterologous expression system, it still may regulate $Na_v1.5$ through proteins of its macromolecular complex.

## Conclusions

We confirmed that 14-3-3η forms a macromolecular complex with human $Na_v1.5$ in a heterologous expression system. Difopein is a potent tool to antagonize 14-3-3-ligand interactions but not the direct physical interaction between two $Na_v1.5$ α-subunits. Overexpression of 14-3-3η did not affect the current mediated by $Na_v1.5$, while difopein potentiated $I_{Na}$ without affecting $Na_v1.5$ total and cell surface expression.

Overall, the role of 14-3-3 proteins on the functionality of $Na_v1.5$ is likely indirect.

## Author contributions

O.I, D.R.K., J.S.R., and H.A. designed this research project. O.I., A.F.H., E.R., A.S, D.R.K., N.S., M.E., S.G., and J.S.R. performed the experiments. O.I., A.F.H., and J.S.R. analyzed the data. O.I. and A.F.H. made Fig.s and tables. O.I. drafted and edited the manuscript. O.I., J.S.R., and H.A. critically reviewed the manuscript.

## Disclosure statement

The authors declare no potential conflict of interest.

## Funding

This work was funded by the Swiss National Science Foundation [SNF 310030_184783] to H.A.

## Acknowledgments

We thank Zoja Selimi (University of Bern) and Jan Kucera (University of Bern) for their invaluable insights and fruitful discussions.

## References

1. Dong, C., Wang, Y., Ma, A. & Wang, T. Life Cycle of the Cardiac Voltage-Gated Sodium Channel NaV1.5. *Front. Physiol.* **11**, 1–11 (2020).
2. Obsil, T. & Obsilova, V. Structural basis of 14-3-3 protein functions. *Semin. Cell Dev. Biol.* **22**, 663–672 (2011).
3. Yang, X. *et al.* Structural basis for protein-protein interactions in the 14-3-3 protein family. *Proc. Natl. Acad. Sci. U. S. A.* **103**, 17237–17242 (2006).
4. Thompson, W. C. & Goldspink, P. H. 14–3-3 Protein Regulation of Excitation–

Contraction Coupling. *Pflugers Arch. Eur. J. Physiol.* 267–279 (2022) doi:10.1007/s00424-021-02635-x.

5. Wang, B. *et al.* Isolation of high-affinity peptide antagonists of 14-3-3 proteins by phage display. *Biochemistry* **38**, 12499–12504 (1999).

6. Henriksson, M. L. *et al.* A nonphosphorylated 14-3-3 binding motif on exoenzyme S that is functional in vivo. *Eur. J. Biochem.* **269**, 4921–4929 (2002).

7. Masters, S. C. & Fu, H. 14-3-3 Proteins Mediate an Essential Anti-apoptotic Signal. *J. Biol. Chem.* **276**, 45193–45200 (2001).

8. Gittenberger-de Groot, A. C. *et al.* 14-3-3Epsilon Controls Multiple Developmental Processes in the Mouse Heart. *Dev. Dyn.* **245**, 1107–1123 (2016).

9. Kosaka, Y. *et al.* 14-3-3ε Plays a Role in Cardiac Ventricular Compaction by Regulating the Cardiomyocyte Cell Cycle. *Mol. Cell. Biol.* **32**, 5089–5102 (2012).

10. Martens, M. D. *et al.* Misoprostol treatment prevents hypoxia-induced cardiac dysfunction through a 14-3-3 and PKA regulatory motif on Bnip3. *Cell Death Dis.* **12**, (2021).

11. Menzel, J. *et al.* 14-3-3 binding creates a memory of kinase action by stabilizing the modified state of phospholamban. **1436**, (2020).

12. Allouis, M. *et al.* 14-3-3 Is a regulator of the cardiac voltage-gated sodium channel Nav1.5. *Circ. Res.* **98**, 1538–1546 (2006).

13. Xing, H., Zhang, S., Weinheimer, C., Kovacs, A. & Muslin, A. J. 14-3-3 Proteins block apoptosis and differentially regulate MAPK cascades. *EMBO J.* **19**, 349–358 (2000).

14. Clatot, J. *et al.* Voltage-gated sodium channels assemble and gate as dimers. *Nat. Commun.* **8**, 1–14 (2017).

15. Yaffe, M. B. How do 14-3-3 proteins work? - Gatekeeper phosphorylation and the molecular anvil hypothesis. *FEBS Lett.* **513**, 53–57 (2002).

16. Gavillet, B. *et al.* Cardiac sodium channel Nav1.5 is regulated by a multiprotein complex composed of syntrophins and dystrophin. *Circ. Res.* **99**, 407–414 (2006).

17. Pohl, P., Joshi, R., Petrvalska, O., Obsil, T. & Obsilova, V. 14-3-3-protein regulates Nedd4-2 by modulating interactions between HECT and WW domains. *Commun. Biol.* **4**, (2021).

18. Van Bemmelen, M. X. *et al.* Cardiac voltage-gated sodium channel Nav1.5 is regulated by Nedd4-2 mediated ubiquitination. *Circ. Res.* **95**, 284–291 (2004).

19. Rougier, J. S. *et al.* Molecular determinants of voltage-gated sodium channel regulation by the Nedd4/Nedd4-like proteins. *Am. J. Physiol. - Cell Physiol.* **288**, 692–701 (2005).

20. Mathew, D. E., Larsen, K., Janeczek, P. & Lewohl, J. M. Expression of 14-3-3

transcript isoforms in response to ethanol exposure and their regulation by miRNAs. *Mol. Cell. Neurosci.* **75**, 44–49 (2016).

21. Utrilla, R. G. *et al.* Kir2.1-Nav1.5 channel complexes are differently regulated than Kir2.1 and Nav1.5 channels alone. *Front. Physiol.* **8**, 1–16 (2017).

22. Abdrabou, A., Brandwein, D. & Wang, Z. Differential subcellular distribution and translocation of seven 14-3-3 isoforms in response to EGF and during the cell cycle. *Int. J. Mol. Sci.* **21**, 1–24 (2020).

23. Iqbal, S. M. & Lemmens-Gruber, R. Phosphorylation of cardiac voltage-gated sodium channel: Potential players with multiple dimensions. *Acta Physiol.* **225**, 1–18 (2019).

24. Abriel, H. Cardiac sodium channel Nav1.5 and interacting proteins: Physiology and pathophysiology. *J. Mol. Cell. Cardiol.* **48**, 2–11 (2010).

25. Kent, C. B. *et al.* 14-3-3 proteins regulate protein kinase A activity to modulate growth cone turning responses. *J. Neurosci.* **30**, 14059–14067 (2010).

26. Aiba, T. *et al.* A mutation causing brugada syndrome identifies a mechanism for altered autonomic and oxidant regulation of cardiac sodium currents. *Circ. Cardiovasc. Genet.* **7**, 249–256 (2014).

27. Psenakova, K. *et al.* 14-3-3 protein directly interacts with the kinase domain of calcium/calmodulin-dependent protein kinase kinase (CaMKK2). *Biochim. Biophys. Acta - Gen. Subj.* **1862**, 1612–1625 (2018).

28. Gannon-Murakami, L. & Murakami, K. Selective association of protein kinase C with 14-3-3 ζ in neuronally differentiated PC12 cells: Stimulatory and inhibitory effect of 14-3-3 ζ in vivo. *J. Biol. Chem.* **277**, 23116–23122 (2002).

29. Galleano, I. *et al.* Functional cross-talk between phosphorylation and disease-causing mutations in the cardiac sodium channel Nav1.5. *Proc. Natl. Acad. Sci. U. S. A.* **118**, (2021).